Hindawi
Shock and Vibration
Volume 2018, Article ID 1697639, 13 pages
https://doi.org/10.1155/2018/1697639

Research Article

Power Flow in a Two-Stage Nonlinear Vibration Isolation System with High-Static-Low-Dynamic Stiffness

Ze-Qi Lu,[1,2] **Dong Shao**,[1,2] **Hu Ding**,[1,2] **and Li-Qun Chen**[1,2,3]

[1]*Shanghai Institute of Applied Mathematics and Mechanics, Shanghai University, Shanghai, China*
[2]*Shanghai Key Laboratory of Mechanics in Energy Engineering, Shanghai University, Shanghai, China*
[3]*Department of Mechanics, Shanghai University, Shanghai, China*

Correspondence should be addressed to Li-Qun Chen; lqchen@staff.shu.edu.cn

Received 17 October 2017; Revised 3 February 2018; Accepted 27 March 2018; Published 15 May 2018

Academic Editor: Toshiaki Natsuki

The manuscript concerns the power flow characterization in a two-stage nonlinear vibration isolator comprising three springs, which are configured so that each stage of the system has a high-static-low-dynamic stiffness. To demonstrate the distinction of evaluation for vibration isolation using power flow, force transmissibility is used for comparison. The dynamic behavior of the isolator subject to harmonic excitation, however, is of interest here. The harmonic balance method (HBM) could be used to analyze the frequency response curve (FRC) of the strong nonlinear vibration system. A suggested stability analysis to distinguish the stable and the unstable HBM solutions is described. Increasing both upper and lower nonlinear stiffness could bend the first resonant peak to the left. The isolation range in the power and the force transmissibility plot could be extended to the lower frequencies when the nonlinear stiffness is increased, but the rate of roll-off for the power transmissibility is twice the rate for the force transmissibility at each horizontal stiffness setting. An explanation for this phenomenon is given in the paper.

1. Introduction

Power flow could be used to quantify the isolation performance and reflect more information of the dynamical system [1–6]. In many cases, the mounting base was flexible. There exists a strong coupling effect between the isolator and the foundation structure [2, 4]. Sciulli and Inman [5] designed a linear vibration isolator for a vibration system supported on the flexible base. The strong interaction between the modes was concerned. More than one mode could be decayed by this damped mount. Later, many literatures concerned the usage of power flow in quantifying the nonlinear vibration isolation with flexible base [7–9].

Vibration isolation with high-static-low-dynamic stiffness (HSLDS) was widely concerned [10–21]. For that, the linear isolation can only occur when the excitation frequency is above $\sqrt{2}\times$ natural frequency of the system. To increase isolation region, the natural frequency of the system needs to be set as low as possible. This can be achieved by a low dynamic stiffness. But the low dynamic stiffness could cause a large static deflection, which is undesirable. This problem can be overcome by a high-static-low-dynamic stiffness (HSLDS). However, single-stage vibration isolation remains a limitation on single-stage vibration isolators' performance, regardless of having the linear or the nonlinear vibration isolation. That is, the transmissibility at which vibration isolation occurs reduces at a maximum rate of 40 dB/decade. This problem can be overcome by the two-stage nonlinear vibration isolation [22]. In this case, the maximum roll-off rate of the transmissibility doubled. Lu et al. [22, 23] investigated a two-stage nonlinear isolator to promote the HSLDS mechanism. HSLDS in each stage has a profound positive effect on isolation performance. In presence of the nonlinearity, the response at the lower natural frequency bends to right but at the second natural frequency it does not. The overall effect of the nonlinearity is to improve the vibration isolation performance compared to a linear two-stage isolator. Wang et al. [24] investigated a two-stage vibration isolation system with quasi-zero stiffness. The isolator with heavy damping in the upper stage, high intermediate mass, and soft spring in the

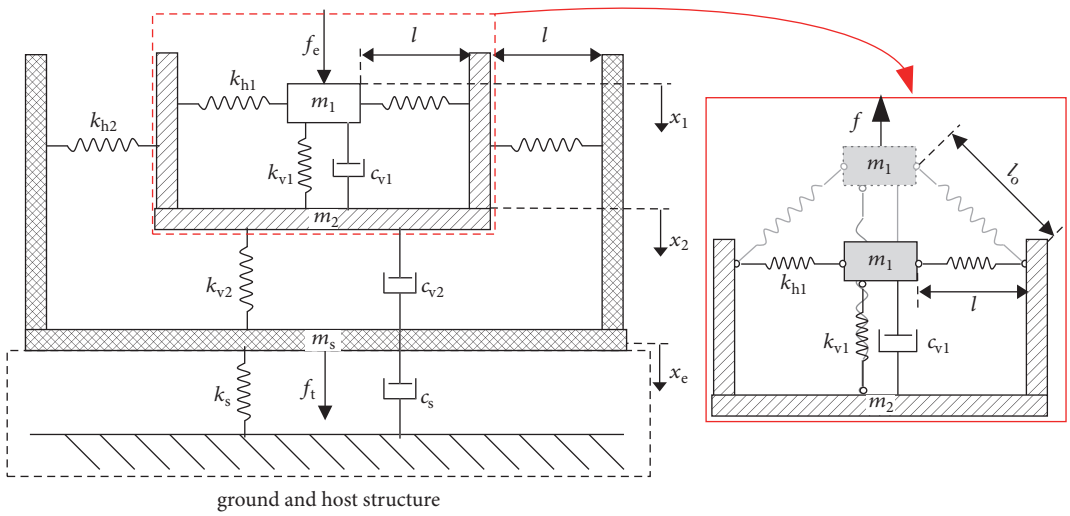

FIGURE 1: Schematic of a two-stage HSLDS vibration isolation system mounted on a linear flexible base. The mass, m_1, is the suspended mass, m_2 is the mass of the intermediate stage, and m_s is the base mass.

lower stage has more desirable advantages. Heavy damping in the upper stage could eliminate the second resonance; thus a broader effective frequency range of isolation can be achieved. Lu et al. [25] experimentally investigated a novel two-stage HSLDS nonlinear vibration isolation system. The positive stiffness in each stage was realized by a metallic plate and the corresponding negative stiffness was realized by a bistable carbon fiber (CF) metal composite plate; a reduction in the displacement transmissibility of about 13 dB at 100 Hz was achieved, compared with the two-stage isolator with the bistable composite plates removed.

To enrich the knowledge of the analysis on the HSLDS vibration isolation and explore the feasibility of the power flow analysis, it is worth studying the behavior of HSLDS vibration isolation systems by power flow analysis. To address the lack of research in these aspects, the present paper focuses on power flow analysis of the two-stage vibration isolation system using HSLDS mechanisms. The harmonic balance method combined with arc-length continuation is used to analyze the power flow of the strong nonlinear vibration. Here, only theoretical model is considered, which explores the advantages of horizontal springs. Alternatively, the horizontal stiffness could be adjusted in practical application, which could overcome the system imperfection caused by mistuning of the mass load. A similar analysis to that conducted in this paper could be carried out for a two-stage HSLDS isolator incorporating such a vertical spring deflection adjustment device [26], but this is outside the scope of the work presented here.

2. Formalizations

Figure 1 shows a two-stage HSLDS vibration system mounted on a linear flexible base. It consists of a primary mass m_1 connected to the secondary mass m_2 that is connected to the flexible base. The oscillators have geometrical nonlinear stiffness; each of the oscillators is modeled by vertical springs k_{v1} and k_{v2}, two horizontal springs k_{h1} and k_{h2}, and vertical dampers c_{v1} and c_{v2}. The linear flexible base consists of a mass m_s, a linear spring with stiffness k_s, and a linear damper with damping c_s.

The stiffness geometrical nonlinearity of the system is generated by the horizontal spring's action in the direction of vertical motion. The total stiffness force of the isolator in each stage can be expressed by

$$f_{\text{upper}} = k_{v1}(x_1 - x_2) + 2k_{h1}\left(1 - \frac{l_o}{\sqrt{(x_1 - x_2)^2 + l^2}}\right)(x_1 - x_2) \tag{1a}$$

$$f_{\text{lower}} = k_{v2}(x_2 - x_s) + 2k_{h2}\left(1 - \frac{l_o}{\sqrt{(x_2 - x_s)^2 + l^2}}\right)(x_2 - x_s) \tag{1b}$$

and the force transfer to the flexible base m_s can be given by

$$f_t = k_{v2}(x_2 - x_s) + 2k_{h2}\left(1 - \frac{l_o}{\sqrt{(x_2 - x_s)^2 + l^2}}\right)(x_2 - x_s) + c_{v2}(\dot{x}_2 - \dot{x}_s), \tag{2}$$

where l_o are the initial lengths of the lateral springs and l are their lengths when they are in the horizontal position. The actual and approximate stiffness terms are very similar for the relatively small motion of the mass where $x_1 \le 0.2l$ and $x_2 \le 0.2l$. In the following analysis, it is therefore assumed that the small displacement (less than about 0.2) approximations

are valid. Note that this is not a severe restriction as the displacements of a practical system are unlikely to be 20% of the length of the horizontal spring. It is also assumed that the maximum value of the excitation force is such that analytical results are valid [12, 23]. Using Taylor expansion, (1a) and (1b) and (2) can be approximated by

$$f_{\text{upper}} = k_{11}\left(x_1 - x_2\right) + k_{13}\left(x_1 - x_2\right)^3 \tag{3a}$$

$$f_{\text{lower}} = k_{21}\left(x_2 - x_s\right) + k_{23}\left(x_2 - x_s\right)^3 \tag{3b}$$

$$\begin{aligned} f_t = {} & k_{21}\left(x_2 - x_s\right) + k_{23}\left(x_2 - x_s\right)^3 \\ & + c_{v2}\left(\dot{x}_2 - \dot{x}_s\right), \end{aligned} \tag{3c}$$

where $k_{11} = k_{v1} - 2(l_o/l - 1)k_{h1}$, $k_{13} = (l_o/l^3)k_{h1}$, $k_{21} = k_{v2} - 2(l_o/l - 1)k_{h2}$, and $k_{23} = (l_o/l^3)k_{h2}$.

The equation of motion for the system in Figure 1 is given by

$$\mathbf{M}\ddot{\mathbf{x}} + \mathbf{C}\dot{\mathbf{x}} + \mathbf{K}\mathbf{x} + \mathbf{K}_3(\mathbf{x}) = \mathbf{f}, \tag{4}$$

where

$$\begin{aligned} \mathbf{M} &= \begin{bmatrix} m_1 & 0 & 0 \\ 0 & m_2 & 0 \\ 0 & 0 & m_s \end{bmatrix}, \\ \mathbf{C} &= \begin{bmatrix} c_{v1} & -c_{v1} & 0 \\ -c_{v1} & c_{v1} + c_{v2} & -c_{v2} \\ 0 & -c_{v2} & c_{v2} + c_s \end{bmatrix}, \\ \mathbf{K} &= \begin{bmatrix} k_{11} & -k_{11} & 0 \\ -k_{11} & k_{11} + k_{21} & -k_{21} \\ 0 & -k_{21} & k_s + k_{21} \end{bmatrix}, \\ \mathbf{x} &= \begin{Bmatrix} x_1 \\ x_2 \\ x_s \end{Bmatrix}, \\ \mathbf{K}_3(\mathbf{x}) &= \begin{Bmatrix} k_{13}\left(x_1 - x_2\right)^3 \\ k_{23}\left(x_2 - x_s\right)^3 - k_{13}\left(x_1 - x_2\right)^3 \\ -k_{23}\left(x_2 - x_s\right)^3 \end{Bmatrix}, \\ \mathbf{f} &= \begin{Bmatrix} F\cos(\omega t) \\ 0 \\ 0 \end{Bmatrix}. \end{aligned} \tag{5}$$

Equation (4) can be written in nondimensional form as

$$\widehat{\mathbf{M}}\hat{\mathbf{x}}'' + \widehat{\mathbf{C}}\hat{\mathbf{x}}' + \widehat{\mathbf{K}}\hat{\mathbf{x}} + \widehat{\mathbf{K}}_3(\hat{\mathbf{x}}) = \hat{\mathbf{f}}, \tag{6}$$

where

$$\widehat{\mathbf{M}} = \begin{bmatrix} 1 & 0 & 0 \\ 0 & \mu_1 & 0 \\ 0 & 0 & \mu_2 \end{bmatrix},$$

$$\widehat{\mathbf{C}} = 2\begin{bmatrix} \zeta_{v1} & -\zeta_{v1} & 0 \\ -\zeta_{v1} & \zeta_{v1} + \mu_1\lambda_1\zeta_{v2} & -\mu_1\lambda_1\zeta_{v2} \\ 0 & -\mu_1\lambda_1\zeta_{v2} & \mu_1\lambda_1\zeta_{v2} + \mu_2\lambda_2\zeta_s \end{bmatrix},$$

$$\hat{\mathbf{x}} = \begin{Bmatrix} \hat{x}_1 \\ \hat{x}_2 \\ \hat{x}_s \end{Bmatrix},$$

$$\widehat{\mathbf{K}} = \begin{bmatrix} \hat{k}_{11} & -\hat{k}_{11} & 0 \\ -\hat{k}_{11} & \hat{k}_{11} + \hat{k}_{21} & -\hat{k}_{21} \\ 0 & -\hat{k}_{21} & \hat{k}_s + \hat{k}_{21} \end{bmatrix},$$

$$\widehat{\mathbf{F}} = \begin{Bmatrix} \hat{k}_{13}\left(\hat{x}_1 - \hat{x}_2\right)^3 \\ \hat{k}_{23}\left(\hat{x}_2 - \hat{x}_s\right)^3 - \hat{k}_{13}\left(\hat{x}_1 - \hat{x}_2\right)^3 \\ -\hat{k}_{23}\left(\hat{x}_2 - \hat{x}_s\right)^3 \end{Bmatrix},$$

$$\hat{\mathbf{f}} = \begin{Bmatrix} \hat{F}\cos(\Omega\tau) \\ 0 \\ 0 \end{Bmatrix},$$

$$x_0 = \left(l_{01}^2 - l_1^2\right)^{1/2},$$

$$\hat{x}_1 = \frac{x_1}{x_0},$$

$$\hat{x}_2 = \frac{x_2}{x_0},$$

$$\hat{x}_s = \frac{x_s}{x_0},$$

$$\mu_1 = \frac{m_2}{m_1},$$

$$\mu_2 = \frac{m_s}{m_1},$$

$$\omega_1 = \sqrt{\frac{k_{v1}}{m_1}},$$

$$\omega_2 = \sqrt{\frac{k_{v2}}{m_2}},$$

$$\omega_s = \sqrt{\frac{k_s}{m_s}},$$

$$\lambda_1 = \frac{\omega_2}{\omega_1},$$

$$\lambda_2 = \frac{\omega_s}{\omega_1},$$
$$\widehat{k}_{11} = 1 - 2\left(\frac{1}{\widehat{l}} - 1\right)\widehat{k}_{h1},$$
$$\widehat{k}_{21} = \widehat{k}_{v2} - 2\left(\frac{1}{\widehat{l}} - 1\right)\widehat{k}_{h2},$$
$$\widehat{k}_{13} = \frac{1 - \widehat{l}^2}{\widehat{l}^3}\widehat{k}_{h1},$$
$$\widehat{k}_{23} = \frac{1 - \widehat{l}^2}{\widehat{l}^3}\widehat{k}_{h2},$$
$$\widehat{k}_s = \frac{k_s}{k_v},$$
$$\widehat{k}_{h1} = \frac{k_{h1}}{k_{v1}},$$
$$\widehat{k}_{v2} = \frac{k_{v2}}{k_{v1}},$$
$$\widehat{k}_{h2} = \frac{k_{h2}}{k_{v1}},$$
$$\zeta_{v1} = \frac{c_{v1}}{2m_1\omega_1},$$
$$\zeta_{v2} = \frac{c_{v2}}{2m_2\omega_2},$$
$$\zeta_s = \frac{c_s}{2m_s\omega_s},$$
$$\widehat{l} = \frac{l}{l_o},$$
$$\widehat{F} = \frac{F}{k_{v1}x_0},$$
$$\Omega = \frac{\omega}{\omega_1}. \tag{7}$$

and $\tau = \omega_1 t$, which is the time scale used for dimensionless treatment [13]. By the dimensionless method, ωt is replaced by $\Omega\tau$, and $(\cdot)' = d(\cdot)/d\tau$.

3. Power Flow Characteristics

3.1. Harmonic Balance Method. Using the HBM, the vector of nondimensional displacement can be assumed as a solution of the form

$$\widehat{\mathbf{x}} = \begin{Bmatrix} \sum_{k=1}^{m} \left(A_{1k}\cos(k\Omega\tau) + A_{2k}\sin(k\Omega\tau)\right) \\ \sum_{k=1}^{m} \left(B_{1k}\cos(k\Omega\tau) + B_{2k}\sin(k\Omega\tau)\right) \\ \sum_{k=1}^{m} \left(D_{1k}\cos(k\Omega\tau) + D_{2k}\sin(k\Omega\tau)\right) \end{Bmatrix}. \tag{8}$$

The high-order harmonics ($m > 3$) are neglected. The result of the amplitude-frequency response can be written as a group of the nonlinear algebraic equations, which could be given in the implicit form as

$$g_i\left(\Omega, A_{11}, A_{21}, A_{13}, A_{23}, B_{11}, B_{21}, B_{13}, B_{23}, D_{11}, D_{21}, D_{13}, D_{23}, \mu_1, \mu_2, \lambda_1, \lambda_2, \zeta_{v1}, \zeta_{v2}, \zeta_{n1}, \zeta_{n2}, \widehat{k}_{11}, \widehat{k}_{21}, \widehat{k}_{13}, \widehat{k}_{23}\right) = 0 \quad i = 1 \cdots 12. \tag{9}$$

The transmitted force is given by

$$\widehat{f}_t(\tau) = \widehat{k}_{21}\left(\widehat{x}_2 - \widehat{x}_s\right) + \widehat{k}_{23}\left(\widehat{x}_2 - \widehat{x}_s\right)^3 + 2\mu_1\zeta_{v2}\lambda_1\left(\widehat{x}_2' - \widehat{x}_s'\right). \tag{10}$$

The force transmissibility defined as the ratio of the root mean square of the transmitted force to the excitation force is given by

$$T_F = 20\log_{10}\left(\frac{\mathrm{RMS}\left(\widehat{f}_t(\tau)\right)}{\mathrm{RMS}\left(\widehat{f}_e(\tau)\right)}\right). \tag{11}$$

The nondimensional instantaneous excited power into the system is the product of the excitation force with the corresponding velocity; it yields

$$p_{in}(\tau) = \widehat{x}_1'(\tau)\,\widehat{f}_e(\tau). \tag{12}$$

The excited power has higher-order harmonics rather than only foundational harmonic; thus the magnitude of the excited power can be determined by root mean square (RMS) of the excited power; this yields

$$P_{in} = \mathrm{RMS}\left(\widehat{x}_1'(\tau)\,\widehat{f}_e(\tau)\right). \tag{13}$$

For vibration isolation, the interest is the amount of power transmission from the vibration source to the flexible base; the nondimensional instantaneous transmitted power is the product of the transmitted force with the corresponding velocity; this yields

$$p_t(\tau) = \widehat{x}_s'(\tau)\,\widehat{f}_t(\tau). \tag{14}$$

The magnitude of the transmitted power is given as the same way in (14):

$$P_t = \mathrm{RMS}\left(\widehat{x}_s'(\tau)\,\widehat{f}_t(\tau)\right). \tag{15}$$

To quantify the effectiveness of the isolation system, power transmissibility may be introduced and defined as the ratio of the transmitted power to the input power; this yields

$$T_P = 20\log_{10}\left(\frac{P_t}{P_{in}}\right). \tag{16}$$

3.2. Stability Analysis. The fundamental harmonic solution can be written as

$$\widehat{\mathbf{x}}^{*} = \begin{Bmatrix} \widehat{x}_1^{*}(\tau) \\ \widehat{x}_2^{*}(\tau) \\ \widehat{x}_s^{*}(\tau) \end{Bmatrix} = \begin{Bmatrix} A_{11}(\tau)\cos(\Omega\tau) + A_{21}(\tau)\sin(\Omega\tau) \\ B_{11}(\tau)\cos(\Omega\tau) + B_{21}(\tau)\sin(\Omega\tau) \\ D_{11}(\tau)\cos(\Omega\tau) + D_{21}(\tau)\sin(\Omega\tau) \end{Bmatrix}. \tag{17}$$

The first and second derivatives of (17) versus τ yield

$$\widehat{\mathbf{x}}'^{*} = \begin{Bmatrix} \widehat{x}_1'^{*}(\tau) \\ \widehat{x}_2'^{*}(\tau) \\ \widehat{x}_s'^{*}(\tau) \end{Bmatrix} = \begin{Bmatrix} \left(A'_{11} + \Omega A_{21}\right)\cos(\Omega\tau) + \left(A'_{21} - \Omega A_{11}\right)\sin(\Omega\tau) \\ \left(B'_{11} + \Omega B_{21}\right)\cos(\Omega\tau) + \left(B'_{21} - \Omega B_{11}\right)\sin(\Omega\tau) \\ \left(D'_{11} + \Omega D_{21}\right)\cos(\Omega\tau) + \left(D'_{21} - \Omega D_{11}\right)\sin(\Omega\tau) \end{Bmatrix}, \tag{18}$$

$$\widehat{\mathbf{x}}''^{*} = \begin{Bmatrix} \widehat{x}_1''^{*}(\tau) \\ \widehat{x}_2''^{*}(\tau) \\ \widehat{x}_s''^{*}(\tau) \end{Bmatrix} = \begin{Bmatrix} \left(A''_{11} + 2\Omega A'_{21} - \Omega^2 A_{11}\right)\cos(\Omega\tau) + \left(A''_{21} - 2\Omega A'_{11} - \Omega^2 A_{21}\right)\sin(\Omega\tau) \\ \left(B''_{11} + 2\Omega B'_{21} - \Omega^2 B_{11}\right)\cos(\Omega\tau) + \left(B''_{21} - 2\Omega B'_{11} - \Omega^2 B_{21}\right)\sin(\Omega\tau) \\ \left(D''_{11} + 2\Omega D'_{21} - \Omega^2 D_{11}\right)\cos(\Omega\tau) + \left(D''_{21} + 2\Omega D'_{11} - \Omega^2 D_{21}\right)\sin(\Omega\tau) \end{Bmatrix}. \tag{19}$$

Substituting (17), (18), and (19) into (8) and equating the coefficient of $\cos(\Omega\tau)$ and $\sin(\Omega\tau)$ to zero lead to six differential-algebraic equations with HBM solution as fixed points.

$$A''_{11} + 2\Omega A'_{21} - \Omega^2 A_{11} + F\left(A_{11}, A_{21}, B_{11}, B_{21}, A'_{11}, A'_{21}, B'_{11}, B'_{21}, \zeta_{v1}, \widehat{k}_{11}, \widehat{k}_{13}, \Omega\right) = 0 \tag{20a}$$

$$A''_{21} - 2\Omega A'_{11} - \Omega^2 A_{21} + F\left(A_{11}, A_{21}, B_{11}, B_{21}, A'_{11}, A'_{21}, B'_{11}, B'_{21}, \zeta_{v1}, \widehat{k}_{11}, \widehat{k}_{13}, \Omega\right) = 0 \tag{20b}$$

$$\mu_1 B''_{11} + 2\mu_1\Omega B'_{21} - \mu_1\Omega^2 B_{11} + F\left(\mu_1, A_{11}, A_{21}, B_{11}, B_{21}, D_{11}, D_{21}, A'_{11}, A'_{21}, B'_{11}, B'_{21}, D'_{11}, D'_{21}, \zeta_{v1}, \zeta_{v2}, \widehat{k}_{11}, \widehat{k}_{21}, \widehat{k}_{13}, \widehat{k}_{23}, \lambda_1, \Omega\right) = 0 \tag{20c}$$

$$\mu_1 B''_{21} - 2\mu_1\Omega B'_{11} - \mu_1\Omega^2 B_{21} + F\left(\mu_1, A_{11}, A_{21}, B_{11}, B_{21}, D_{11}, D_{21}, A'_{11}, A'_{21}, B'_{11}, B'_{21}, D'_{11}, D'_{21}, \zeta_{v1}, \zeta_{v2}, \widehat{k}_{11}, \widehat{k}_{21}, \widehat{k}_{13}, \widehat{k}_{23}, \lambda_1, \Omega\right) = 0 \tag{20d}$$

$$\mu_2 D''_{11} + 2\mu_2\Omega D'_{21} - \mu_2\Omega^2 D_{11} + F\left(\mu_1, \mu_2, B_{11}, B_{21}, D_{11}, D_{21}, B'_{11}, B'_{21}, D'_{11}, D'_{21}, \zeta_s, \zeta_{v2}, \widehat{k}_s, \widehat{k}_{13}, \widehat{k}_{23}, \lambda_1, \lambda_2, \Omega\right) = 0 \tag{20e}$$

$$\mu_2 D''_{21} - 2\mu_2\Omega D'_{11} - \mu_2\Omega^2 D_{21} + F\left(\mu_1, \mu_2, B_{11}, B_{21}, D_{11}, D_{21}, B'_{11}, B'_{21}, D'_{11}, D'_{21}, \zeta_s, \zeta_{v2}, \widehat{k}_s, \widehat{k}_{13}, \widehat{k}_{23}, \lambda_1, \lambda_2, \Omega\right) = 0. \tag{20f}$$

$\widehat{\mathbf{x}}^{*}$ is HBM solution; $\Delta\widehat{\mathbf{x}}$ is the deviation value of the HBM solution, so

$$\widehat{\mathbf{x}} = \widehat{\mathbf{x}}^{*} + \Delta\widehat{\mathbf{x}}, \tag{21}$$

where

$$\Delta\mathbf{x} = \begin{Bmatrix} \Delta A_{11}\cos(\Omega\tau) + \Delta A_{21}\sin(\Omega\tau) \\ \Delta B_{11}\cos(\Omega\tau) + \Delta B_{21}\sin(\Omega\tau) \\ \Delta D_{11}\cos(\Omega\tau) + \Delta D_{21}\sin(\Omega\tau) \end{Bmatrix}. \tag{22}$$

Linearizing the six differential-algebraic equations at the fixed points gives perturbation equation:

$$\mathbf{I}\mathbf{u}'' + \mathbf{C}\mathbf{u}' + \mathbf{K}\mathbf{u} = \mathbf{0}, \tag{23}$$

where

$$\mathbf{u}'' = \begin{bmatrix} \Delta A''_{11} \\ \Delta A''_{21} \\ \Delta B''_{11} \\ \Delta B''_{21} \\ \Delta D''_{11} \\ \Delta D''_{21} \end{bmatrix},$$

$$\mathbf{I} = \begin{bmatrix} 1 & 0 & 0 & 0 & 0 & 0 \\ 0 & 1 & 0 & 0 & 0 & 0 \\ 0 & 0 & \mu_1 & 0 & 0 & 0 \\ 0 & 0 & 0 & \mu_1 & 0 & 0 \\ 0 & 0 & 0 & 0 & \mu_2 & 0 \\ 0 & 0 & 0 & 0 & 0 & \mu_2 \end{bmatrix},$$

$$\mathbf{u}' = \begin{bmatrix} \Delta A'_{11} \\ \Delta A'_{21} \\ \Delta B'_{11} \\ \Delta B'_{21} \\ \Delta D'_{11} \\ \Delta D'_{21} \end{bmatrix},$$

$$\mathbf{u} = \begin{bmatrix} \Delta A_{11} \\ \Delta A_{21} \\ \Delta B_{11} \\ \Delta B_{21} \\ \Delta D_{11} \\ \Delta D_{21} \end{bmatrix},$$

$$\mathbf{C} = \begin{bmatrix} 2\zeta_{v1} & 2\Omega & -2\zeta_{v1} & 0 & 0 & 0 \\ -2\Omega & 2\zeta_{v1} & 0 & -2\zeta_{v1} & 0 & 0 \\ -2\zeta_{v1} & 0 & 2\zeta_{v2}\lambda_1\mu_1 + 2\zeta_{v1} & 2\mu_1\Omega & -2\zeta_{v2}\lambda_1\mu_1 & 0 \\ 0 & -2\zeta_{v1} & -2\mu_1\Omega & 2\zeta_{v2}\lambda_1\mu_1 + 2\zeta_{v1} & 0 & -2\zeta_{v2}\lambda_1\mu_1 \\ 0 & 0 & -2\zeta_{v2}\lambda_1\mu_1 & 0 & 2\zeta_s\lambda_2\mu_2 + 2\zeta_{v2}\lambda_1\mu_1 & 2\mu_2\Omega \\ 0 & 0 & 0 & -2\zeta_{v2}\lambda_1\mu_1 & -2\mu_2\Omega & 2\zeta_s\lambda_2\mu_2 + 2\zeta_{v2}\lambda_1\mu_1 \end{bmatrix}$$

$$\mathbf{K} = \begin{bmatrix} K_{11} & K_{12} & K_{13} & K_{14} & K_{15} & K_{16} \\ K_{21} & K_{22} & K_{23} & K_{24} & K_{25} & K_{26} \\ K_{31} & K_{32} & K_{33} & K_{34} & K_{35} & K_{36} \\ K_{41} & K_{42} & K_{43} & K_{44} & K_{45} & K_{46} \\ K_{51} & K_{52} & K_{53} & K_{54} & K_{55} & K_{56} \\ K_{61} & K_{62} & K_{63} & K_{64} & K_{65} & K_{66} \end{bmatrix},$$

$$K_{11} = k_{11} - \Omega^2 + k_{13}\left(\frac{3}{4}B_{21}^2 + \frac{9}{4}B_{11}^2 + \frac{3}{4}A_{21}^2 + \frac{9}{4}A_{11}^2 - \frac{9}{2}A_{11}B_{11} - \frac{3}{2}A_{21}B_{21}\right)$$

$$K_{12} = \frac{3}{2}k_{13}\left(B_{11}B_{21} + A_{11}A_{21} - A_{11}B_{21} - A_{21}B_{11}\right)$$

$$K_{13} = -k_{11} + k_{13}\left(-\frac{3}{4}B_{21}^2 - \frac{9}{4}B_{11}^2 - \frac{3}{4}A_{21}^2 - \frac{9}{4}A_{11}^2 + \frac{9}{2}A_{11}B_{11} + \frac{3}{2}A_{21}B_{21}\right)$$

$$K_{14} = \frac{3}{2}k_{13}\left(-B_{11}B_{21} - A_{11}A_{21} + A_{11}B_{21} + A_{21}B_{11}\right)$$

$$K_{15} = 0$$

$$K_{16} = 0$$

$$K_{21} = \frac{3}{2}k_{13}\left(A_{11}A_{21} - A_{11}B_{21} + B_{11}B_{21} - A_{21}B_{11}\right)$$

$$K_{22} = k_{11} - \Omega^2 + k_{13}\left(\frac{3}{4}A_{11}^2 + \frac{9}{4}A_{21}^2 + \frac{3}{4}B_{11}^2 + \frac{9}{4}B_{21}^2 - \frac{9}{2}A_{21}B_{21} - \frac{3}{2}A_{11}B_{11}\right)$$

$$K_{23} = \frac{3}{2}k_{13}\left(A_{11}B_{21} + A_{21}B_{11} - A_{11}A_{21} - B_{11}B_{21}\right)$$

$$K_{24} = -k_{11} + k_{13}\left(-\frac{3}{4}A_{11}^2 - \frac{9}{4}A_{21}^2 - \frac{3}{4}B_{11}^2 - \frac{9}{4}B_{21}^2 + \frac{9}{2}A_{21}B_{21} + \frac{3}{2}A_{11}B_{11}\right)$$

$$K_{25} = 0$$

$$K_{26} = 0$$

$$K_{31} = -k_{11} - k_{13}\left(\frac{3}{4}B_{21}^2 + \frac{9}{4}B_{11}^2 + \frac{3}{4}A_{21}^2 + \frac{9}{4}A_{11}^2 - \frac{9}{2}A_{11}B_{11} - \frac{3}{2}A_{21}B_{21}\right)$$

$$K_{32} = -\frac{3}{2}k_{13}\left(B_{11}B_{21} + A_{11}A_{21} - A_{11}B_{21} - A_{21}B_{11}\right)$$

$$K_{33} = k_{21} - \mu_1\Omega^2 + k_{11} - k_{13}\left(-\frac{3}{4}B_{21}^2 - \frac{9}{4}B_{11}^2 - \frac{3}{4}A_{21}^2 - \frac{9}{4}A_{11}^2 + \frac{9}{2}A_{11}B_{11} + \frac{3}{2}A_{21}B_{21}\right)$$
$$+ k_{23}\left(\frac{3}{4}D_{21}^2 + \frac{9}{4}D_{11}^2 + \frac{3}{4}B_{21}^2 + \frac{9}{4}B_{11}^2 - \frac{9}{2}B_{11}D_{11} - \frac{3}{2}B_{21}D_{21}\right)$$

$$K_{34} = \frac{3}{2}k_{23}\left(D_{11}D_{21} + B_{11}B_{21} - B_{11}D_{21} - B_{21}D_{11}\right) - \frac{3}{2}k_{13}\left(-B_{11}B_{21} - A_{11}A_{21} + A_{11}B_{21} + A_{21}B_{11}\right)$$

$$K_{35} = -k_{21} + k_{23}\left(-\frac{3}{4}D_{21}^2 - \frac{9}{4}D_{11}^2 - \frac{3}{4}B_{21}^2 - \frac{9}{4}B_{11}^2 + \frac{9}{2}B_{11}D_{11} + \frac{3}{2}B_{21}D_{21}\right)$$

$$K_{36} = \frac{3}{2}k_{23}\left(-D_{11}D_{21} - B_{11}B_{21} + B_{11}D_{21} + B_{21}D_{11}\right)$$

$$K_{41} = -\frac{3}{2}k_{13}\left(A_{11}A_{21} - A_{11}B_{21} + B_{11}B_{21} - A_{21}B_{11}\right)$$

$$K_{42} = -k_{11} - k_{13}\left(\frac{3}{4}A_{11}^2 + \frac{9}{4}A_{21}^2 + \frac{3}{4}B_{11}^2 + \frac{9}{4}B_{21}^2 - \frac{9}{2}A_{21}B_{21} - \frac{3}{2}A_{11}B_{11}\right)$$

$$K_{43} = \frac{3}{2}k_{23}\left(B_{11}B_{21} - B_{11}D_{21} + D_{11}D_{21} - B_{21}D_{11}\right) - \frac{3}{2}k_{13}\left(A_{11}B_{21} + A_{21}B_{11} - A_{11}A_{21} - B_{11}B_{21}\right)$$

$$K_{44} = k_{21} + k_{11} - \mu_1\Omega^2 + k_{23}\left(\frac{3}{4}B_{11}^2 + \frac{9}{4}B_{21}^2 + \frac{3}{4}D_{11}^2 + \frac{9}{4}D_{21}^2 - \frac{9}{2}B_{21}D_{21} - \frac{3}{2}B_{11}D_{11}\right)$$
$$- k_{13}\left(-\frac{3}{4}A_{11}^2 - \frac{9}{4}A_{21}^2 - \frac{3}{4}B_{11}^2 - \frac{9}{4}B_{21}^2 + \frac{9}{2}A_{21}B_{21} + \frac{3}{2}A_{11}B_{11}\right)$$

$$K_{45} = \frac{3}{2}k_{23}\left(B_{11}D_{21} + B_{21}D_{11} - B_{11}B_{21} - D_{11}D_{21}\right)$$

$$K_{46} = -k_{21} + k_{23}\left(-\frac{3}{4}B_{11}^2 - \frac{9}{4}B_{21}^2 - \frac{3}{4}D_{11}^2 - \frac{9}{4}D_{21}^2 + \frac{9}{2}B_{21}D_{21} + \frac{3}{2}B_{11}D_{11}\right)$$

$$K_{51} = 0$$

$$K_{52} = 0$$

$$K_{53} = -k_{21} + k_{23}\left(-\frac{3}{4}D_{21}^2 - \frac{9}{4}D_{11}^2 - \frac{3}{4}B_{21}^2 - \frac{9}{4}B_{11}^2 + \frac{9}{2}B_{11}D_{11} + \frac{3}{2}B_{21}D_{21}\right)$$

$$K_{54} = \frac{3}{2}k_{23}\left(-D_{11}D_{21} - B_{11}B_{21} + B_{11}D_{21} + B_{21}D_{11}\right)$$

$$K_{55} = k_s + k_{21} - \mu_2\Omega^2 + k_{23}\left(\frac{3}{4}D_{21}^2 + \frac{9}{4}D_{11}^2 + \frac{3}{4}B_{21}^2 + \frac{9}{4}B_{11}^2 - \frac{9}{2}B_{11}D_{11} - \frac{3}{2}B_{21}D_{21}\right)$$

$$
\begin{aligned}
K_{56} &= \frac{3}{2}k_{23}\left(D_{11}D_{21} + B_{11}B_{21} - B_{11}D_{21} - B_{21}D_{11}\right)\\
K_{61} &= 0\\
K_{62} &= 0\\
K_{63} &= \frac{3}{2}k_{23}\left(B_{11}B_{21} - B_{11}D_{21} + D_{11}D_{21} - B_{21}D_{11}\right)\\
K_{64} &= -k_{21} + k_{23}\left(-\frac{3}{4}B_{11}^2 - \frac{9}{4}B_{21}^2 - \frac{3}{4}D_{11}^2 - \frac{9}{4}D_{21}^2 + \frac{9}{2}B_{21}D_{21} + \frac{3}{2}B_{11}D_{11}\right)\\
K_{65} &= \frac{3}{2}k_{23}\left(-D_{11}D_{21} - B_{11}B_{21} + B_{11}D_{21} + B_{21}D_{11}\right)\\
K_{66} &= k_s + k_{21} - \mu_2\Omega^2 + k_{23}\left(\frac{3}{4}B_{11}^2 + \frac{9}{4}B_{21}^2 + \frac{3}{4}D_{11}^2 + \frac{9}{4}D_{21}^2 - \frac{9}{2}B_{21}D_{21} - \frac{3}{2}B_{11}D_{11}\right).
\end{aligned}
\tag{24}
$$

Eigenvalues can be determined by

$$\left|\theta^2\mathbf{I} + \theta\mathbf{C} + \mathbf{K}\right| = \mathbf{0}, \tag{25}$$

where θ is the eigenvalue, the coefficients in the linearized perturbation equation A_{11}, A_{21}, B_{11}, B_{21}, D_{11}, and D_{21} can be determined by (9). Equation (9) is a group of the nonlinear algebraic equations. These unknown parameters A_{11}, A_{21}, B_{11}, B_{21}, D_{11}, and D_{21} can be calculated by Newton iteration method. Calculate the eigenvalues to determine the stability. If the real part of the eigenvalue is negative, the HBM solution is stable. If the real part of the eigenvalue is positive, the HBM solution is unstable.

3.3. Results and Discussion. To check whether the method of harmonic balance correctly calculates the frequency response curve for the parameters chosen, the amplitudes of the displacement of the primary, the secondary, and the base mass are plotted in Figure 2 together with numerical method using Runge-Kutta scheme. The mass ratio 1 : 0.2 : 1 is chosen in this case. The numerical solutions in the figures are shown as black "o." The analytical and the numerical results perfectly agree in the stable portions and so the method of harmonic balance can be used for further investigation of the dynamic behavior. The unstable solution shown as a red dotted line cannot be validated as this solution cannot be reached by numerical integration of the equations of motion.

This article addressed the positive effects of using horizontal stiffness in the two stages. The horizontal stiffnesses in two stages are the same, $\widehat{k}_{\mathrm{h1}} = \widehat{k}_{\mathrm{h2}}$. Such assumption is convenient to analyze the problem but does not affect the results of the analysis of this article. Indeed, the comparison of the effects of the horizontal stiffness between upper and lower stages may be desirable. An analytical method to that conducted in this paper could be applied when the horizontal stiffnesses between upper and lower stages are different, but this is outside the scope of the work presented here.

To demonstrate the reduction of the power through the two-stage nonlinear vibration isolator, input and transmitted power are plotted together in Figure 3(a), with $\widehat{k}_{\mathrm{h1}} = \widehat{k}_{\mathrm{h2}} = 0.9$. It can be observed that the power is reduced dramatically in almost all ranges of the frequencies except the frequencies around the resonance. Figure 3(b) illustrates the comparison of power transmissibility between the two-stage HSLDS isolator, the two-stage linear HSLDS isolator, the single-stage HSLDS isolator, and the single-stage linear isolator. The linear isolators with horizontal stiffness removed are used for comparison. Horizontal stiffness could enlarge the vibration isolation bandwidth. Power transmissibility of the two-stage isolator is reduced at higher roll-off rate compared with the single-stage isolator. Of particular interest, the two-stage linear isolator outperforms the single-stage HSLDS isolator.

A parameter study was carried out to investigate how changes in the nonlinear stiffness, mass ratio, and length ratio can affect the power flow. Figure 4(a) shows the effects on the power transmissibility when horizontal stiffness is changed. It can be seen that the power transmissibility peak bends to the right around the first natural frequency but the peaks around the second and the third natural frequency do not. Increasing upper and lower stage horizontal stiffness can extend the isolation range to the lower frequencies and improve the vibration isolation performance. Figure 4(b) shows the effects on force transmissibility when horizontal stiffness is changed. Force transmissibility peak shifts to the lower frequencies when upper and lower stage horizontal stiffness is increased. For high frequency, the rate of roll-off for the power transmissibility is twice the rate for the force transmissibility at each horizontal stiffness setting. Analysis of the definitions of the power and force transmissibility can give the reason for this. From (25), derive

$$
\begin{aligned}
T_{\mathrm{P}} &= 20\log_{10}\left(\frac{\mathrm{RMS}\left(\widehat{\dot{x}}_{\mathrm{s}}'(\tau)\,\widehat{f}_{\mathrm{t}}(\tau)\right)}{\mathrm{RMS}\left(\widehat{\dot{x}}_{1}'(\tau)\,\widehat{f}_{\mathrm{e}}(\tau)\right)}\right)\\
&= 20\log_{10}\left(\frac{\mathrm{RMS}\left(\widehat{\dot{x}}_{\mathrm{s}}'(\tau)\right)\mathrm{RMS}\left(\widehat{f}_{\mathrm{t}}(\tau)\right)}{\mathrm{RMS}\left(\widehat{\dot{x}}_{1}'(\tau)\right)\mathrm{RMS}\left(\widehat{f}_{\mathrm{e}}(\tau)\right)}\right)
\end{aligned}
$$

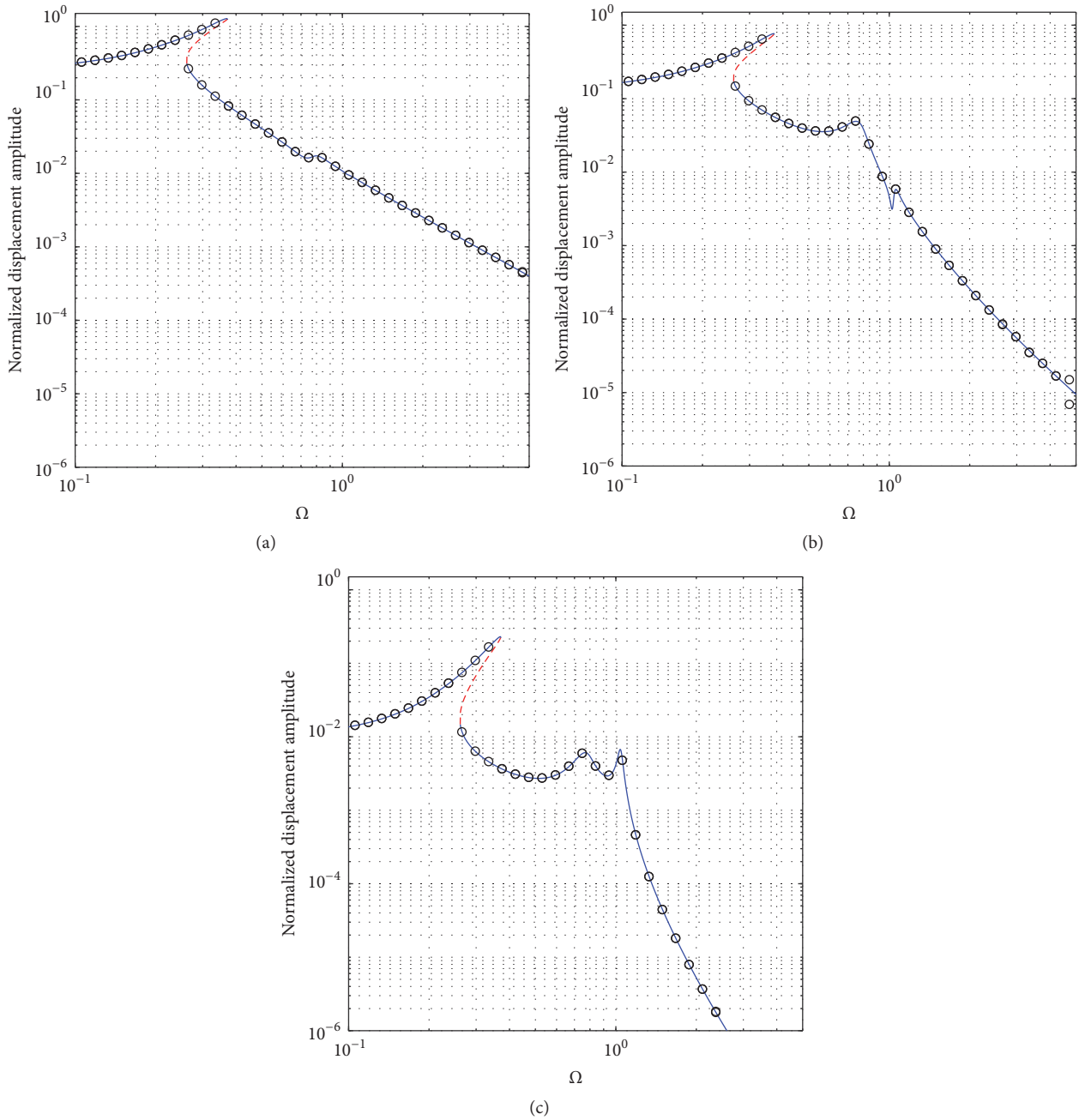

FIGURE 2: The frequency response curve (FRC) of the two-stage HSLDS isolation system. The parameters are $\mu_1 = 0.2$, $\mu_2 = 1$, $\lambda_1 = \sqrt{5}$, $\lambda_2 = 1$, $\widehat{k}_s = 1$, $\widehat{k}_{h1} = \widehat{k}_{h2} = 0.9$, $\widehat{l} = 0.7$, $\widehat{F} = 0.01$, and $\zeta_{v1} = \zeta_{v2} = \zeta_s = 0.01$. (a) FRC of m_1, (b) FRC of m_2, and (c) FRC of m_s. HBM solution: stable solution (blue line) and unstable solution (red dashed line). Numerical solution: black "o."

$$= 20\log_{10}\left(\frac{\mathrm{RMS}\left(\Omega\widehat{x}_s(\tau+\pi/2)\right)}{\mathrm{RMS}\left(\Omega\widehat{x}_1(\tau+\pi/2)\right)}\cdot\frac{\mathrm{RMS}\left(\widehat{f}_t(\tau)\right)}{\mathrm{RMS}\left(\widehat{f}_e(\tau)\right)}\right)$$
$$= 20\log_{10}\left(\frac{\mathrm{RMS}\left(\widehat{x}_s(\tau+\pi/2)\right)}{\mathrm{RMS}\left(\widehat{x}_1(\tau+\pi/2)\right)}\right)$$
$$+ 20\log_{10}\left(\frac{\mathrm{RMS}\left(\widehat{f}_t(\tau)\right)}{\mathrm{RMS}\left(\widehat{f}_e(\tau)\right)}\right) = T_D + T_F, \quad (26)$$

where T_D is the displacement transmissibility. For high frequency excitation, the displacement transmissibility equals the force transmissibility as shown in [23]. So, (26) becomes

$$T_P = 2T_F. \quad (27)$$

For low frequency, there is a new peak before the first resonance peak in power transmissibility plot. The reason for this is that the relative displacement at the high-order natural frequency between the upper and the lower masses

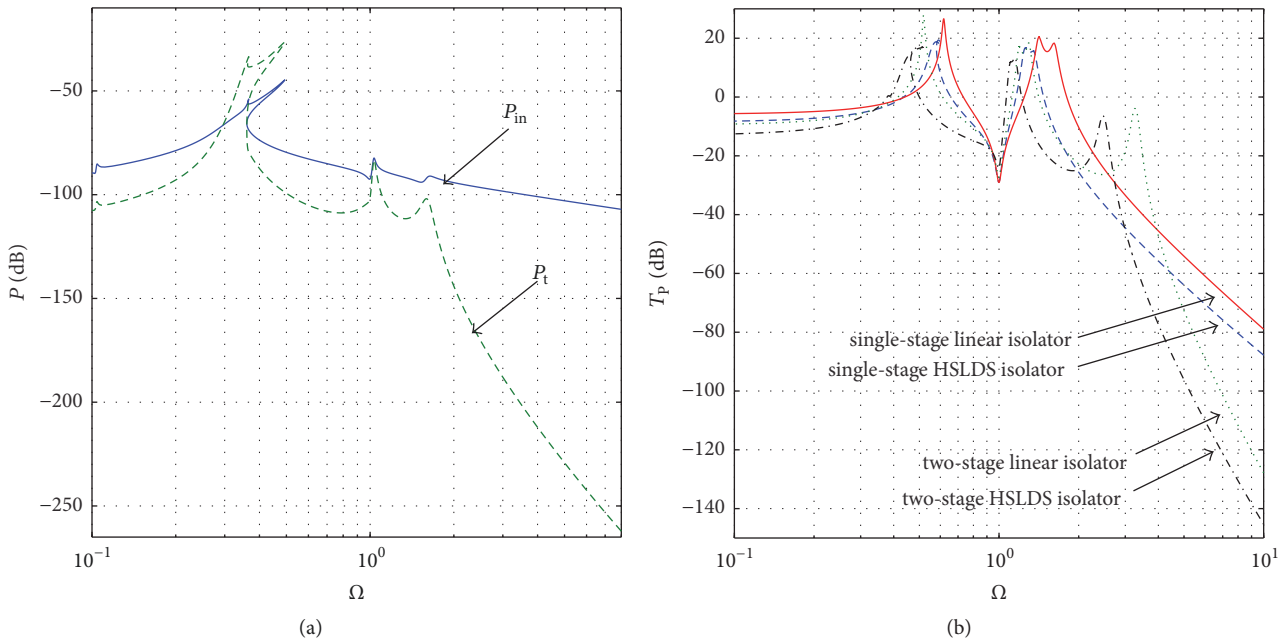

FIGURE 3: Power flow in the two-stage isolation system. The parameters are $\mu_1 = 0.2$, $\mu_2 = 1$, $\lambda_1 = \sqrt{5}$, $\lambda_2 = 1$, $\hat{k}_s = 1$, $\hat{k}_{h1} = \hat{k}_{h2} = 0.9$, $\hat{l} = 0.7$, $\hat{F} = 0.01$, and $\zeta_{v1} = \zeta_{v2} = \zeta_s = 0.01$. (a) Comparison of power P between upper mass m_1 and base mass m_s. (b) Comparison of the power transmissibility T_P between the single-stage linear, the single-stage HSLDS, two-stage linear, and two-stage HSLDS isolators.

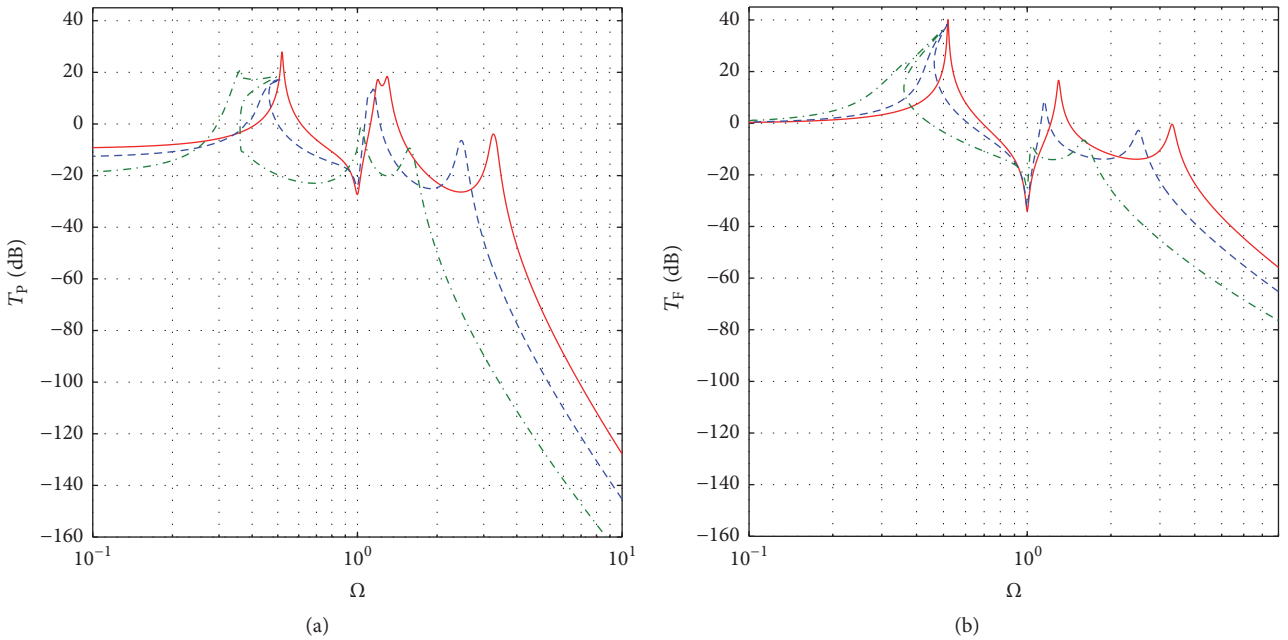

FIGURE 4: Power transmissibility (a) and force transmissibility (b) of the two-stage HSLDS system with different horizontal stiffness ($\hat{k}_{h1}, \hat{k}_{h2}$). The parameters are $\mu_1 = 0.2$, $\mu_2 = 1$, $\lambda_1 = \sqrt{5}$, $\lambda_2 = 1$, $\hat{k}_s = 1$, $\hat{l} = 0.7$, $\hat{F} = 0.01$, and $\zeta_{v1} = \zeta_{v2} = \zeta_s = 0.01$. Red solid line is shown as the linear system; blue dashed line, $\hat{k}_{h1} = \hat{k}_{h2} = 0.5$; green dashed-dotted line, $\hat{k}_{h1} = \hat{k}_{h2} = 0.9$.

and between the lower mass and the base is small, as is the displacement of the base, so the nonlinear effects on the power flow are minimal at this frequency. However, the relative displacement is relatively large at the first resonance frequency and so the nonlinear effect is more significant at this frequency. This is why the first resonant frequency for the power flow is affected much more by the horizontal springs, as seen in Figure 4. The effects of the mass ratio and length are investigated, respectively, when the two-stage isolator has only horizontal stiffness fixed at $\hat{k}_{h1} = \hat{k}_{h2} = 0.9$. Figure 5

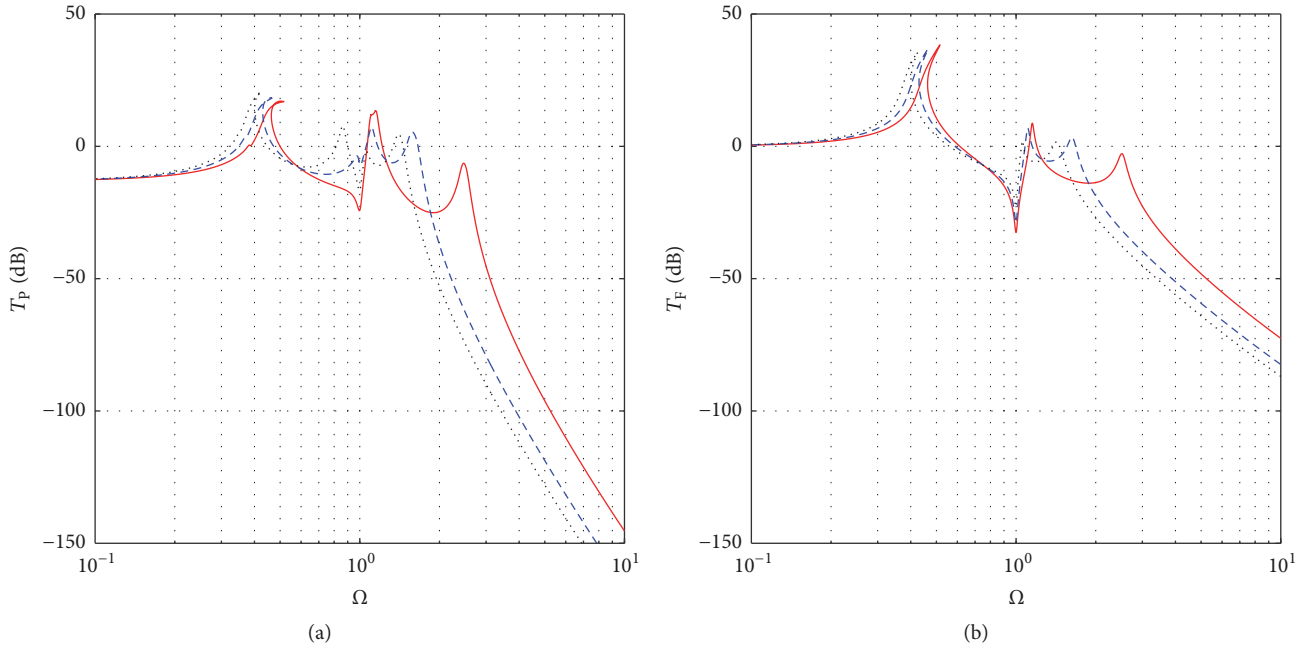

FIGURE 5: Power transmissibility (a) and force transmissibility (b) of the two-stage HSLDS system with different mass ratio μ_1. The parameters are $\mu_2 = 1$, $\lambda_1 = \sqrt{5}$, $\lambda_2 = 1$, $\widehat{k}_s = 1$, $\widehat{k}_{h1} = \widehat{k}_{h2} = 0.9$, $\widehat{l} = 0.7$, $\widehat{F} = 0.01$, and $\zeta_{v1} = \zeta_{v2} = \zeta_s = 0.01$. Red solid line is shown as the mass ratio $\mu_1 = 0.2$; blue dashed line, $\mu_1 = 0.6$; black-dotted line, $\mu_1 = 1$.

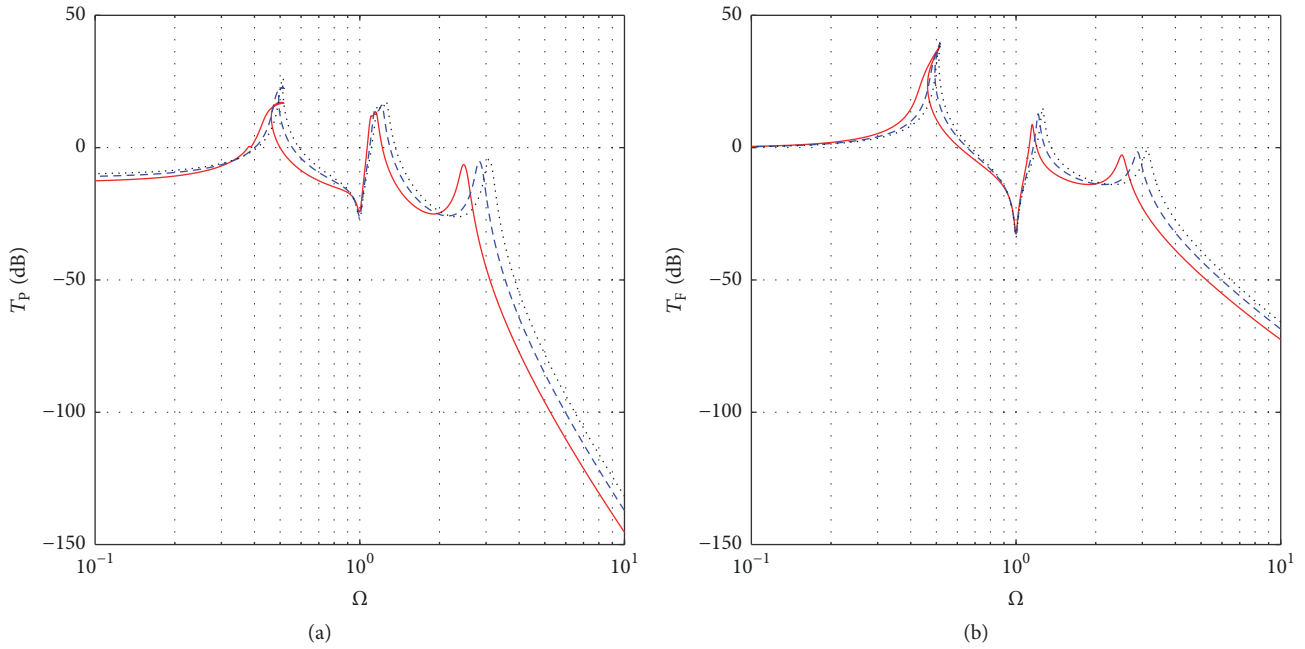

FIGURE 6: Power transmissibility (a) and force transmissibility (b) of the two-stage HSLDS system with different ratio of $\widehat{l}$. The parameters are $\mu_1 = 0.2$, $\mu_2 = 1$, $\lambda_1 = \sqrt{5}$, $\lambda_2 = 1$, $\widehat{k}_s = 1$, $\widehat{k}_{h1} = \widehat{k}_{h2} = 0.9$, $\widehat{F} = 0.01$, and $\zeta_{v1} = \zeta_{v2} = \zeta_s = 0.01$. Red solid line is shown as the ratio $\widehat{l} = 0.7$; blue dashed line, $\widehat{l} = 0.8$; black-dotted line, $\widehat{l} = 0.9$.

shows the effects on the power and force transmissibility when mass ratio is changed in the two-stage isolator. The second peak shifts to the lower frequencies but the first peak remains almost the same, when μ_1 is increased. Magnitudes of the force transmissibility are reduced significantly at high frequencies. Figure 6 shows the variations of the power and force transmissibility against the length ratio. It can be seen that peaks of both power and force transmissibility shift to lower

frequencies, the isolation region is extended to lower frequencies, but the frequency for the antiresonance is not affected.

As shown in Figures 3–6 for the examples' simulations, some benefits on practical applications could be explored. Increasing nonlinear stiffness can extend the isolation range to the lower frequencies and improve the vibration isolation performance. Mass ratio and length ratio can enhance the benefits of the nonlinearity. The parameter setting is derived from the model of the artificial satellite vibration isolation. These results could give general rules for the designing of the vibration isolation of artificial satellite.

4. Conclusions

In this manuscript, power flow of a two-stage nonlinear isolator mounted on a linear flexible base has been investigated. Both the input and transmitted power frequency responses are considered. The vertical stiffness in the both stages is superposition of the horizontal stiffness that acts as negative stiffness. Hence, the natural frequency is reduced. The effects of the resulting nonlinear isolator have then been investigated. It has been found that the first resonant peak in the input and transmitted power frequency response curve bends to the left when increasing the horizontal stiffness in both stages. The overall effects of the nonlinearity on power flow are to improve the vibration isolation designing compared with linear system.

Conflicts of Interest

The authors declare that there are no potential conflicts of interest with respect to the research, authorship, and/or publication of this article.

Acknowledgments

This work was supported by the State Key Program of National Natural Science Foundation of China (no. 11232009), the National Natural Science Foundation of China (nos. 11502135 and 11572182), and the Innovation Program of Shanghai Municipal Education Commission (no. 2017-01-07-00-09-E00019).

References

[1] J. T. Xing, *Energy Flow Theory of Nonlinear Dynamical Systems with Applications*, Springer, Switzerland, 2015.

[2] Y. P. Xiong, J. T. Xing, and W. G. Price, "Interactive power flow characteristics of an integrated equipment - Nonlinear isolator - Travelling flexible ship excited by sea waves," *Journal of Sound and Vibration*, vol. 287, no. 1-2, pp. 245–276, 2005.

[3] G. Kerschen, M. Peeters, J. C. Golinval, and A. F. Vakakis, "Nonlinear normal modes, Part I: A useful framework for the structural dynamicist," *Mechanical Systems and Signal Processing*, vol. 23, no. 1, pp. 170–194, 2009.

[4] J. Yang, Y. P. Xiong, and J. T. Xing, "Nonlinear power flow analysis of the Duffing oscillator," *Mechanical Systems and Signal Processing*, vol. 45, no. 2, pp. 563–578, 2014.

[5] D. Sciulli and D. J. Inman, "Isolation design for a flexible system," *Journal of Sound and Vibration*, vol. 216, no. 2, pp. 251–267, 1998.

[6] M. Guzmán-Nieto, P. E. Tapia-González, and D. F. Ledezma-Ramírez, "Low frequency experimental analysis of dry friction damping in cable isolators," *Journal of Low Frequency Noise, Vibration and Active Control*, vol. 34, no. 4, pp. 513–524, 2015.

[7] J. Yang, Y. P. Xiong, and J. T. Xing, "Dynamics and power flow behaviour of a nonlinear vibration isolation system with a negative stiffness mechanism," *Journal of Sound and Vibration*, vol. 332, no. 1, pp. 167–183, 2013.

[8] J. Yang, Y. P. Xiong, and J. T. Xing, "Vibration power flow and force transmission behaviour of a nonlinear isolator mounted on a nonlinear base," *International Journal of Mechanical Sciences*, vol. 115-116, pp. 238–252, 2016.

[9] Z. Xia, X. Wang, J. Hou, S. Wei, and Y. Fang, "Non-linear dynamic analysis of double-layer semi-active vibration isolation systems using revised Bingham model," *Journal of Low Frequency Noise, Vibration and Active Control*, vol. 35, no. 1, pp. 17–24, 2016.

[10] A. Valeev, A. Zotov, and S. Kharisov, "Designing of compact low frequency vibration isolator with quasi-zero-stiffness," *Journal of Low Frequency Noise, Vibration and Active Control*, vol. 34, no. 4, pp. 459–474, 2015.

[11] D. Ning, S. Sun, J. Zhang, H. Du, W. Li, and X. Wang, "An active seat suspension design for vibration control of heavy-duty vehicles," *Journal of Low Frequency Noise, Vibration and Active Control*, vol. 35, no. 4, pp. 264–278, 2016.

[12] A. Carrella, M. J. Brennan, T. P. Waters, and V. Lopes Jr., "Force and displacement transmissibility of a nonlinear isolator with high-static-low-dynamic-stiffness," *International Journal of Mechanical Sciences*, vol. 55, no. 1, pp. 22–29, 2012.

[13] A. Carrella, M. J. Brennan, and T. P. Waters, "Static analysis of a passive vibration isolator with quasi-zero-stiffness characteristic," *Journal of Sound and Vibration*, vol. 301, no. 3–5, pp. 678–689, 2007.

[14] A. Carrella, *Passive Vibration Isolators with High-Static-Low-Dynamic-Stiffness*, University of Southampton, UK, 2008.

[15] P. Alabuzhev, A. Gritchin, L. Kim, G. Migirenko, V. Chon, and P. Stepanov, *Vibration Protecting and Measuring Systems with Quasi-Zero Stiffness*, Hemisphere Publishing, NY, USA, 1989.

[16] A. Carrella, M. J. Brennan, and T. P. Waters, "Optimization of a quasi-zero-stiffness isolator," *Journal of Mechanical Science and Technology*, vol. 21, no. 6, pp. 946–949, 2007.

[17] X. Sun, X. Jing, L. Cheng, and J. Xu, "A 3-D quasi-zero-stiffness-based sensor system for absolute motion measurement and application in active vibration control," *IEEE/ASME Transactions on Mechatronics*, vol. 20, no. 1, pp. 254–262, 2015.

[18] C.-C. Lan, S.-A. Yang, and Y.-S. Wu, "Design and experiment of a compact quasi-zero-stiffness isolator capable of a wide range of loads," *Journal of Sound and Vibration*, vol. 333, no. 20, pp. 4843–4858, 2014.

[19] G. Dong, X. Zhang, S. Xie, B. Yan, and Y. Luo, "Simulated and experimental studies on a high-static-low-dynamic stiffness isolator using magnetic negative stiffness spring," *Mechanical Systems and Signal Processing*, vol. 86, pp. 188–203, 2017.

[20] Y. Zheng, X. Zhang, Y. Luo, B. Yan, and C. Ma, "Design and experiment of a high-static-low-dynamic stiffness isolator using a negative stiffness magnetic spring," *Journal of Sound and Vibration*, vol. 360, pp. 31–52, 2016.

[21] C. Cheng, S. Li, Y. Wang, and X. Jiang, "Force and displacement transmissibility of a quasi-zero stiffness vibration isolator with geometric nonlinear damping," *Nonlinear Dynamics*, vol. 87, no. 4, pp. 2267–2279, 2017.

[22] Z. Lu, M. J. Brennan, T. Yang, X. Li, and Z. Liu, "An investigation of a two-stage nonlinear vibration isolation system," *Journal of Sound and Vibration*, vol. 322, no. 4-5, pp. 1456–1464, 2013.

[23] Z. Lu, T. Yang, M. J. Brennan, X. Li, and Z. Liu, "On the Performance of a Two-Stage Vibration Isolation System Which has Geometrically Nonlinear Stiffness," *ASME Journal of Vibration and Acoustics*, vol. 136, no. 6, p. 064501, 2014.

[24] X. Wang, J. Zhou, D. Xu, H. Ouyang, and Y. Duan, "Force transmissibility of a two-stage vibration isolation system with quasi-zero stiffness," *Nonlinear Dynamics*, vol. 87, no. 1, pp. 633–646, 2017.

[25] Z. Lu, Y. Tiejun, M. J. Brennan, Z. Liu, and L.-Q. Chen, "Experimental Investigation of a Two-Stage Nonlinear Vibration Isolation System with High- Static-Low-Dynamic Stiffness," *ASME Journal of Applied Mechanics*, vol. 84, no. 2, Article ID 021001, 2017.

[26] Y. Wang, S. Li, S. A. Neild, and J. Z. Jiang, "Comparison of the dynamic performance of nonlinear one and two degree-of-freedom vibration isolators with quasi-zero stiffness," *Nonlinear Dynamics*, vol. 88, no. 1, pp. 635–654, 2017.